

**SYNTHESIS, FORMATION AND
CHARACTERIZATION OF NANOSCALE
ZEOLITE TYPE W BASE CATALYST**

CHEONG YING WAI

UNIVERSITI SAINS MALAYSIA

2021

**SYNTHESIS, FORMATION AND
CHARACTERIZATION OF NANOSCALE
ZEOLITE TYPE W BASE CATALYST**

by

CHEONG YING WAI

**Thesis submitted in fulfilment of the requirement
for the degree of
Doctor of Philosophy**

March 2021

ACKNOWLEDGEMENT

First and foremost, I would like to express my greatest gratitude to my supervisor Assoc. Prof. Dr. Ng Eng Poh for his guidance, valuable opinions and assistance throughout this project. His in-depth knowledge and expertise in zeolite science has helped bringing this project to fruition without which would not have been this successful. I would also like to thank the School of Chemical Sciences, Universiti Sains Malaysia (USM) and Université de Caen for sharing their analytical resources and technical support. Not to forget, special thanks to RUI (1001/PKIMIA/8011012) grant, Bridging Fund (304/PKIMIA/6316006 and 304/PKIMIA/6316506), and FRGS (203/PKIMIA/6711642) grant and USM fellowship for providing financial support and scholarship. I would also like to extend my gratitude to all academic and non-academic staff of School of Chemical Sciences, USM who have provided assistance during my PhD candidature. Many thanks to my teammates, Ms. Hidayahni, Dr. Tamara, Dr. Ghadah, Mr. Ismail and Dr. Haruna for their constructive discussions and helpfulness over the course of this project. Last but not least, I would like to express my deep appreciation to my family who have always been supportive in my pursuit of postgraduate studies for this work could not have been completed without their immense moral and mental support.

TABLE OF CONTENTS

ACKNOWLEDGEMENT.....	ii
TABLE OF CONTENTS.....	iii
LIST OF TABLES.....	viii
LIST OF FIGURES.....	ix
LIST OF SYMBOLS AND NOMENCLATURES.....	xvii
ABSTRAK.....	xxi
ABSTRACT.....	xxii
CHAPTER 1 INTRODUCTION.....	1
1.1 General introduction.....	1
1.2 Research objectives.....	3
1.3 Scope of thesis.....	4
CHAPTER 2 LITERATURE REVIEW.....	7
2.1 Zeolites.....	7
2.2 History of zeolites.....	9
2.3 Synthesis of zeolites.....	11
2.3.1 Source of T elements.....	11
2.3.2 Structure-directing agents (SDAs).....	12
2.3.3 Mineralizer.....	13
2.3.4 Solvent.....	14
2.4 Merlinoite zeolite.....	15
2.4.1 Structure of MER framework.....	15
2.4.2 Synthesis of MER zeolite.....	17
2.4.3 Applications of MER zeolite.....	20
2.5 Nanoscale zeolite.....	21
2.5.1 Nanosized zeolites in zeolite membrane.....	22
2.5.2 Nanosized zeolites in sensors.....	22
2.5.3 Nanosized zeolites in biological and medical applications.....	23
2.6 Synthesis of nanosized zeolites.....	23
2.7 Zeolite formation mechanism.....	25

2.7.1	Nucleation and growth of zeolites in dense precursor gel.....	26
2.7.2	Nucleation and growth of zeolites in clear suspensions.....	27
2.8	Zeolite as catalyst.....	28
2.9	Cyanoethylation between acrylonitrile and alcohol.....	29
2.10	Knoevenagel condensation between aldehyde/ketone and active methylene compound.....	31
2.11	Henry reaction between aldehyde and nitroalkane.....	32
2.12	Heating method.....	34
2.12.1	Microwave heating.....	34
2.12.2	Non-microwave instant heating.....	36
CHAPTER 3	MATERIALS AND EXPERIMENTAL METHODS.....	38
3.1	Introduction.....	38
3.2	Chemicals.....	38
3.3	Effects of synthesis parameters on crystallization behavior of K-W zeolite.....	39
3.4	Crystal growth study of nanosized K-W zeolite from bamboo leaves ash.....	41
3.5	Rapid synthesis of nanocrystalline zeolite K-W with hierarchical mesoporosity.....	42
3.6	Characterization.....	43
3.6.1	X-ray Powder diffraction (XRD) analysis.....	43
3.6.2	Fourier-transform infrared (FTIR) spectroscopy.....	45
3.6.3	Solid-state magic-angle spinning nuclear magnetic resonance spectroscopy (MAS NMR).....	46
3.6.4	Field emission scanning electron microscopy (FESEM).....	49
3.6.5	Transmission electron microscopy (TEM).....	51
3.6.6	Inductively coupled plasma-optical emission spectrometry (ICP-OES).....	53

3.6.7	Nitrogen (N ₂) gas adsorption-desorption analysis.....	54
3.6.8	Temperature-programmed desorption (TPD).....	57
3.6.9	Gas chromatography (GC) analysis.....	58
3.6.10	Gas chromatography-mass spectrometry (GC-MS) analysis.....	60
3.7	Study of catalytic behaviour of K-W nano-zeolite.....	61
3.7.1	Henry reaction of benzaldehyde and 1-nitropropane.....	61
3.7.2	Cyanoethylation between methanol and acrylonitrile.....	62
3.7.3	Knoevenagel condensation of benzaldehyde and ethyl cyanoacetate.....	63
CHAPTER 4	EFFECTS OF SYNTHESIS PARAMETERS ON CRYSTALLIZATION BEHAVIOR OF K-W ZEOLITE.....	64
4.1	Introduction.....	64
4.2	Results and discussion.....	65
4.2.1	Effect of SiO ₂ content.....	65
4.2.2	Effect of water content.....	70
4.2.3	Effect of K ₂ O content.....	73
4.2.4	Effect of heating temperature.....	77
4.2.5	Effect of heating time.....	79
4.2.6	Morphological effects on the surface basicity of zeolite.....	82
4.3	Summary.....	86
CHAPTER 5	CRYSTAL GROWTH STUDY OF NANOSIZED K-W ZEOLITE FROM BAMBOO LEAVES ASH.....	87
5.1	Introduction.....	87
5.2	Results and discussion.....	88
5.2.1	Crystallization kinetics study of K-W nanozeolite.....	88

5.2.2	Microscopic observation of crystallization of K-W nanozeolite.....	92
5.2.3	Growth mechanism of K-W zeolite nanocrystals	98
5.3	Summary.....	101
CHAPTER 6	RAPID SYNTHESIS OF NANOCRYSTALLINE ZEOLITE W WITH HIERARCHICAL MESOPOROSITY.....	102
6.1	Introduction.....	102
6.2	Results and discussion.....	103
6.2.1	Synthesis and crystal growth of nanosized K-W zeolite.....	103
6.2.2	Effect of metal cations in directing zeolite framework.....	104
6.2.3	Microscopic study of K-W zeolite nanocrystals	105
6.2.4	Chemical environment of Al and Si atoms in the K-W nanozeolites.....	107
6.2.5	FT-IR spectroscopy analysis.....	109
6.2.6	Nitrogen gas absorption-desorption study.....	110
6.3	Summary.....	112
CHAPTER 7	CATALYTIC BEHAVIOUR STUDIES OF K-W ZEOLITE BASE CATALYST.....	113
7.1	Catalytic study of cyanoethylation between methanol and acrylonitrile.....	113
7.1.1	Effect of morphologies.....	113
7.1.2	Effect of catalyst loading.....	114
7.1.3	Effect of heating temperature and time.....	115
7.1.4	Effect of methanol to acrylonitrile molar ratio...	116
7.1.5	Effect of solvents.....	119
7.1.6	Catalyst reusability test.....	120
7.1.7	Proposed mechanism.....	121
7.2	Catalytic reaction study in Knoevenagel condensation of benzaldehyde and ethyl cyanoacetate.....	124
7.2.1	Effect of catalyst loading.....	124

	7.2.2	Effect of heating temperature and time.....	125
	7.2.3	Effect of benzaldehyde to ethyl cyanoacetate molar ratio.....	126
	7.2.4	Effect of solvents.....	129
	7.2.5	Catalyst comparative study.....	130
	7.2.6	Catalyst reusability test.....	131
	7.2.7	Proposed mechanism.....	132
7.3		Catalytic study of nitroaldol Henry reaction between benzaldehyde and nitropropane.....	135
	7.2.1	Effect of catalyst loading.....	135
	7.2.2	Effect of heating temperature and time.....	136
	7.2.3	Effect of benzaldehyde to nitropropane molar ratio.....	138
	7.2.4	Effect of solvents.....	140
	7.2.5	Catalyst comparative study.....	141
	7.2.6	Catalyst reusability test.....	143
	7.2.7	Proposed mechanism.....	144
7.4		Summary.....	146
		CHAPTER 8 CONCLUSION AND RECOMMENDATIONS.....	147
8.1		Conclusion.....	147
8.2		Recommendation of future works.....	149
		REFERENCES.....	151
		APPENDICES	
		LIST OF PUBLICATIONS	

LIST OF TABLES

		Page
Table 2.1	A comparison of MER zeolite synthesis conditions.....	19
Table 3.1	The chemical compositions of precursor hydrogels and their respective synthesis conditions.....	40
Table 3.2	Possible vibration bands in the fingerprint region of zeolite frameworks (Flanigen, 1974).....	46
Table 3.3	IUPAC classification of pores (Sing, 1991).....	54
Table 3.4	Characteristics of adsorption isotherms (Sing, 1982; Bel Japan Inc, 2013).....	55
Table 3.5	GC oven-programmed setup for studying catalytic reactions..	60
Table 4.1	The chemical compositions of precursor hydrogels and their respective synthesis conditions.....	67
Table 4.2	TPD-CO ₂ basicity of K-W zeolites with various morphologies.....	85
Table 5.1	Chemical composition of solids after progressive hydrothermal heating.....	94
Table 7.1	Effect of solvents on conversion of acrylonitrile ^a	119
Table 7.2	Effect of solvents on conversion of benzaldehyde ^a	129
Table 7.3	Effect of solvents on conversion of benzaldehyde ^a	141

LIST OF FIGURES

		Page
Figure 2.1	The chemical structure of zeolites whereby the negative charge on Al atoms is counter-balanced by the positive charge of metal cations.....	7
Figure 2.2	Secondary building units (SBUs) and their symbols. Number in parentheses indicates frequency of occurrence in zeolite frameworks (Moshoeshoe et al., 2017).....	8
Figure 2.3	Examples of zeolites framework structures: (a) LTA, (b) FAU, (c) MFI and (d) LTL (Zheng et al., 2012).....	11
Figure 2.4	SBUs of MER framework: (a) double-8-ring (D8R), (b) pau unit and (c) double crankshaft chain (Baerlocher & McCusker, 2019).....	15
Figure 2.5	Framework structure of MER zeolite viewed along [001] (Baerlocher & McCusker, 2019).....	16
Figure 2.6	PerBU consisted of (a) 4 crankshaft chains and (b) 4-fold connected D8Rs (Baerlocher & McCusker, 2019).....	16
Figure 2.7	<i>mer</i> cavity (a) viewed along c direction and (b) viewed along b direction (Baerlocher & McCusker, 2019).....	17
Figure 2.8	Four types of 8-membered ring channel systems in MER-type zeolite (Baerlocher & McCusker, 2019).....	17
Figure 2.9	TEM images of (a) LTJ- (b) EDI- (c) ABW- and (d) ANA-type zeolite nanocrystals (Ng et al., 2015b; Wong et al., 2017a; Ghrear et al., 2019; Ng et al., 2019b).....	21
Figure 2.10	Schematic representation of the (a) nucleation rate and (b) crystal growth rates of zeolites where the (b) process is described with a typical S-shaped curve (Grand et al., 2016)....	26
Figure 2.11	Schematic representation of a proposed zeolite growth mechanism from clear precursor suspensions (Grand et al., 2016).....	28
Figure 2.12	Cyanoethylation reaction between acrylonitrile and compound with labile hydrogen atom (Bruson, 2011).....	30

Figure 2.13	Cyanoethylation of methanol with acrylonitrile catalyzed by a base catalyst.....	30
Figure 2.14	Cyanoethylation mechanism of methanol with acrylonitrile catalyzed by homogeneous base catalyst (Feit & Zilkha, 1963; Edenborough, 1999).....	31
Figure 2.15	Examples of active methylene compounds used in Knoevenagel condensation reaction (Tietze & Beifuss, 1991)..	32
Figure 2.16	A general mechanism of Knoevenagel condensation reaction (Khare et al., 2019).....	32
Figure 2.17	A general mechanism of Henry reaction (ScienceDirect, 2021).....	33
Figure 2.18	Henry reaction between nitroalkane and aldehyde/ketone (Luzzio, 2001).....	33
Figure 2.19	Schematic diagram of conventional conductive heating where the temperature of the outside surface is higher than the internal temperature (Hayes, 2002).....	35
Figure 2.20	Principles of microwave heating: (a) dipole disorder without electric field, (b) dipole alignment under continuous electric field, and (c) dipole rotation under high frequency electric field (2.45 GHz) causing internal heating due to molecular dipole instability.....	36
Figure 2.21	Schematic diagram of a non-microwave instant heating reactor (Obermayer, 2016).....	37
Figure 3.1	Schematic diagram of preparation of bamboo leaves to bamboo leaves silica ash (BLA).....	41
Figure 3.2	A simple schematic diagram of X-ray diffractometer.....	44
Figure 3.3	²⁹ Si NMR chemical shift ranges of Si(nAl) species (Stepanov, 2016).....	48
Figure 3.4	Schematic diagram of a FESEM microscope (Gleichmann, 2020).....	50
Figure 3.5	Schematic diagram of a TEM microscope (Gleichmann, 2020).....	52

Figure 3.6	Schematic diagram of an inductively coupled plasma-optical emission spectrometer (Morishige & Kimura, 2008).....	53
Figure 3.7	IUPAC classification of adsorption isotherms (Sing, 1982).....	55
Figure 3.8	Type of hysteresis loops (Sing, 1982).....	56
Figure 3.9	Schematic diagram of a typical GC (McNair et al, 2019).....	58
Figure 3.10	A schematic representation of the chromatographic process (McNair et al, 2019).....	59
Figure 3.11	Schematic diagram of a typical GC-MS system (Mourão et al., 2020).....	60
Figure 4.1	XRD patterns of (a) W-1, (b) W-2, (c) W-3 and (d) W-4 samples crystallized at 180 °C for 14 h using an aluminosilicate gel precursor of $y\text{SiO}_2:1\text{Al}_2\text{O}_3:3.5\text{K}_2\text{O}:130\text{H}_2\text{O}$ where $y = 1.5, 5, 7$ and 10 , respectively. The * marks in (c) indicate the presence of the LTL crystalline phase.....	69
Figure 4.2	FESEM images of solids prepared using a precursor hydrogel of $y\text{SiO}_2:1\text{Al}_2\text{O}_3:3.5\text{K}_2\text{O}:130\text{H}_2\text{O}$ at 180 °C for 14 h where $y =$ (a) 1.5 (W-1), (b) 5 (W-2), (c) 7 (W-3) and (d) 10 (W-4).....	70
Figure 4.3	XRD patterns of (a) W-5, (b) W-3, (c) W-6 and (d) W-7 samples prepared from an aluminosilicate precursor hydrogel with a composition of $7\text{SiO}_2:1\text{Al}_2\text{O}_3:3.5\text{K}_2\text{O}:z\text{H}_2\text{O}$ with $z = 100, 130, 196$ and 280 , respectively. All samples were heated at 180 °C for 14 h. The * marks in (a, b) indicate the presence of the LTL crystalline phase.....	72
Figure 4.4	FESEM images of (a) W-5, (b) W-3, (c) W-6 and (d) W-7 samples solids prepared using a gel precursor of $7\text{SiO}_2:1\text{Al}_2\text{O}_3:3.5\text{K}_2\text{O}:z\text{H}_2\text{O}$ at 180 °C for 14 h where $z = 100, 130, 196$ and 280 , respectively.....	73
Figure 4.5	XRD patterns of samples prepared from an aluminosilicate gel precursor with the composition of $7\text{SiO}_2:1\text{Al}_2\text{O}_3:x\text{K}_2\text{O}:196\text{H}_2\text{O}$ with $x =$ (a) 3.5 (W-6), (b) 5 (W-8) and (c) 7 (W-9). All samples were heated at 180 °C for 14 h.....	75

Figure 4.6	FESEM images of (a) W-6, (b) W-8 and (c) W-9 samples prepared from an aluminosilicate gel precursor with the composition of $7\text{SiO}_2: 1\text{Al}_2\text{O}_3: x\text{K}_2\text{O}: 196\text{H}_2\text{O}$ with $x = 3.5, 5$ and 7 , respectively. The arrows shown in (b) indicate the existence of K-W nanorod crystals in midst of K-W prismatic crystals.....	76
Figure 4.7	XRD patterns of (a) W-10, (b) W-11, (c) W-12 and (d) W-6 samples upon heating at 120, 140, 160 and 180 °C for 14 h, respectively.....	78
Figure 4.8	FESEM images of (a) W-10, (b) W-11, (c) W-12 and (d) W-6 samples upon heating at 120, 140, 160 and 180 °C for 14 h, respectively.....	79
Figure 4.9	XRD patterns of (a) W-13, (b) W-14, (c) W-6 and (d) W-15 samples heated for 0 h, 10 h, 14 h and 20 h, respectively.....	80
Figure 4.10	FESEM images of (a)W-13, (b)W-14, (c)W-6 and (d)W-15 samples heated for 0, 10, 14 and 20 h, respectively.....	81
Figure 4.11	TPD-CO ₂ profiles of (a) nanorod (W-6), (b) bullet-like (W-15), (c) prismatic (W-9), and (d) wheatsheaf-like K-W zeolites (W-7).....	84
Figure 5.1	XRD patterns of samples after heating for (a) 0 h, (b) 1.5 h, (c) 2.3 h, (d) 3.0 h and (e) 6.0 h.....	88
Figure 5.2	Solid yield and degree of crystallinity of solid samples versus hydrothermal treatment times.....	89
Figure 5.3	TEM images of samples after heated for (a, b) 0 h, (c, d) 1.5 h, (e, f) 2.3 h and (g–h) 6.0 h under various magnifications. HRTEM images of samples show (i) clear lattice fringes with an interplanar spacing of 0.35 nm and (j) SAED pattern of K-W zeolite nanocrystals viewed along the [001] zone axis.....	90
Figure 5.4	FTIR spectra of samples after (a) 0 h, (b) 1.5 h, (c) 2.3 h, (d) 3.0 and (e) 6.0 h of heating.....	93
Figure 5.5	²⁷ Al MAS NMR spectra of samples after (a) 0 h, (b) 1.5 h, (c) 2.3 h, (d) 3.0 h and (d) 6.0 h. * indicates spinning sidebands.....	96

Figure 5.6	²⁹ Si MAS NMR spectra of samples after (a) 0 h, (b) 1.5 h, (c) 2.3 h, (d) 3.0 h and (d) 6.0 h.....	97
Figure 5.7	Proposed mechanism of the formation of nanosized K-W zeolite. Inset: Framework structure of solid. Green: Si or Al atom, and red: O atom. K ⁺ ion is excluded for better visualization.....	100
Figure 6.1	XRD patterns of solid samples after microwave irradiation for (a) 2 min, (b) 10 min and (c) 12 min.....	104
Figure 6.2	XRD patterns of (a) simulated ANA crystalline phase, solids synthesized using (b) NaOH and (c) CsOH. The solid samples were synthesized using hydrogels with a molar composition of 1Al ₂ O ₃ :7SiO ₂ :3.5M ₂ O:196H ₂ O (M= Na or Cs) at 180 °C under microwave irradiation (800 W, 12 min).....	105
Figure 6.3	FESEM images with (a) low and (b) high magnifications showing the nanorods morphology of the synthesized K-W crystals with hierarchical porosity.....	106
Figure 6.4	(a–c) HRTEM images showing the nanorods morphology of the synthesized K-W crystals under various magnifications. (d) SAED pattern of nanocrystalline K-W zeolite along the [010] zone axis.....	107
Figure 6.5	²⁷ Al MAS NMR spectra of nanocrystalline K-W zeolite.....	108
Figure 6.6	²⁹ Si MAS NMR spectra of nanocrystalline K-W zeolite.....	108
Figure 6.7	IR spectrum of nanocrystalline K-W zeolite.....	109
Figure 6.8	Nitrogen gas adsorption (close symbols) and desorption (open symbols) isotherms of nanocrystalline K-W zeolite.....	110
Figure 6.9	Nitrogen gas adsorption (closed symbols) and desorption (open symbols) isotherm plots, and pore size distribution curve (inset) of micron-sized K-W (MER topology) zeolite.....	111
Figure 7.1	Catalytic performance of (a) nanorod (W-6), (b) bullet-like (W-15), (c) prismatic (W-9), and (d) wheatsheaf-like (W-7) K-W zeolites on cyanoethylation of methanol. Reaction temperature = 140 °C, 0.5 g of K-W catalyst, methanol:acrylonitrile = 28:7, n = 2.....	114

Figure 7.2	Effect of catalyst (W-6) amount on cyanoethylation reaction. Methanol: acrylonitrile molar ratio = 28:7, heating time = 15 min, reaction temperature = 140 °C, n = 2.....	115
Figure 7.3	Cyanoethylation of methanol and acrylonitrile at (a) 120 °C, (b) 130 °C, and (c) 140 °C. Methanol: acrylonitrile molar ratio = 28:7, 0.5 g of K-W (W-6) catalyst, n = 2.....	116
Figure 7.4	Effect of methanol to acrylonitrile molar ratio on cyanoethylation reaction: (a) increasing concentration of acrylonitrile, and (b) increasing concentration of methanol. Reaction temperature = 140 °C, heating time = 15 min, 0.5 g of K-W (W-6) catalyst, n = 2.....	118
Figure 7.5	Effect of solvents on cyanoethylation reaction. Reaction temperature = 140 °C, heating time = 15 min, 0.5 g of K-W catalyst, methanol:acrylonitrile = 28:7, n = 2.....	120
Figure 7.6	Catalyst reusability test of W-3 nanocrystals in cyanoethylation reaction of methanol and acrylonitrile. Reaction temperature = 140 °C, heating time = 15 min, methanol:acrylonitrile = 28:7, n = 2.....	121
Figure 7.7	A proposed reaction mechanism of cyanoethylation between methanol and acrylonitrile catalyzed by K-W solid base catalyst.....	123
Figure 7.8	Knoevenagel condensation of benzaldehyde and ethyl cyanoacetate.....	124
Figure 7.9	Effect of catalyst amount on Knoevenagel condensation. Benzaldehyde: ethyl cyanoacetate molar ratio = 8:8, heating time = 30 min, reaction temperature = 180 °C, n = 2.....	125
Figure 7.10	Knoevenagel condensation of benzaldehyde and ethyl cyanoacetate at (a) 160 °C, (b) 170 °C, and (c) 180 °C. Benzaldehyde: ethyl cyanoacetate molar ratio = 8:8, 0.50 g of K-W catalyst, n = 2.....	126
Figure 7.11	Effect of benzaldehyde to ethyl cyanoacetate molar ratio (B:EC) on Knoevenagel condensation: (a) increasing equimolar of benzaldehyde and ethyl cyanoacetate, (b)	

	increasing benzaldehyde concentration, and (c) increasing ethyl cyanoacetate concentration. Reaction temperature = 180 °C, heating time = 30 min, 0.50 g of K-W catalyst, n = 2...	128
Figure 7.12	Effect of solvents on Knoevenagel condensation reaction. Reaction temperature = 180 °C, heating time = 30 min, 0.50 g of K-W catalyst, benzaldehyde: ethyl cyanoacetate = 8:8, n = 2.....	130
Figure 7.13	Conversion of benzaldehyde and selectivity to ECP in Knoevenagel condensation using different types of catalysts. Reaction temperature = 180 °C, heating time = 60 min, 0.50 g of K-W catalyst, benzaldehyde: ethyl cyanoacetate = 8:8, n = 2.....	131
Figure 7.14	Catalyst reusability test of K-W nanocrystals in Knoevenagel condensation reaction of benzaldehyde and ethyl cyanoacetate. Reaction temperature = 180 °C, heating time = 60 min, benzaldehyde: ethyl cyanoacetate = 8:8, n = 2.....	132
Figure 7.15	A proposed reaction mechanism of Knoevenagel condensation between benzaldehyde and ethyl cyanoacetate catalyzed by K-W solid base catalyst.....	134
Figure 7.16	Henry reaction of benzaldehyde with nitropropane.....	135
Figure 7.17	Effect of catalyst amount on the benzaldehyde conversion. Benzaldehyde:nitropropane molar ratio = 1:20, heating time = 60 min, reaction temperature = 190 °C, n = 2.....	136
Figure 7.18	Henry reaction of benzaldehyde and nitropropane at (a) 170 °C, (b) 180 °C, and (c) 190 °C. Benzaldehyde:nitropropane molar ratio = 1:20, 0.50 g of K-W catalyst, n = 2.....	137
Figure 7.19	Effect of benzaldehyde to nitropropane (B:NP) molar ratio on the conversion of benzaldehyde: (a) increasing nitropropane concentration and (b) increasing benzaldehyde concentration. Reaction temperature = 190 °C, heating time = 60 min, 0.50 g of K-W catalyst, n = 2.....	139

Figure 7.20	Effect of solvents on the conversion of benzaldehyde. Reaction temperature = 190 °C, heating time = 60 min, 0.50 g of K-W catalyst, benzaldehyde:nitropropane = 1:20, volume of solvents = 1 mL, n = 2.....	141
Figure 7.21	Conversion of benzaldehyde and selectivity to 1-(2-nitrobut-1-enyl)benzene in Henry reaction using different types of catalysts. Reaction temperature = 180 °C, heating time = 40 min, 0.50 g of K-W catalyst, benzaldehyde:nitropropane = 1:20, n = 2.....	142
Figure 7.22	Catalyst reusability test of K-W nanocrystals in Henry reaction of benzaldehyde and nitropropane. Reaction temperature = 190 °C, heating time = 60 min, benzaldehyde:nitropropane = 1:20, n = 2.....	143
Figure 7.23	A proposed reaction mechanism of Henry condensation between benzaldehyde and nitropropane catalyzed by K-W zeolite.....	145

LIST OF SYMBOLS AND NOMENCLATURES

°	Degree
λ	Lambda
θ	Theta
°C	Degree Celcius
μm	Micrometre
Å	Angstrom (1×10^{-10} m)
A	Absorbance
Al	Aluminium
Al^{3+}	Aluminium cation
AlO_4	Aluminium tetraoxide
Al_2O_3	Aluminium oxide
$\text{Al}(\text{OH})_3$	Aluminum hydroxide
ANA	Analcime
B_0	Static magnetic field
Ba^{2+}	Barium cation
BEA	Beta polymorph A
BET	Brunauer-Emmett-Teller
BJH	Barrett-Joyner-Halenda
BLA	Bamboo leaf ash
C	Carbon
ca.	Circa (approximately)
CBU	Composite building unit
CEC	Cation exchange capacity
CCD	Charge-coupled device
CH_4	Methane
CHA	Chabazite
cm	Centimetre
CO_2	Carbon dioxide
Cs^+	Caesium cation
$\text{CsOH} \cdot \text{H}_2\text{O}$	Caesium hydroxide monohydrate
d	Day

D4R	Double four rings
D5R	Double five rings
D6R	Double six rings
D8R	Double eight rings
DMSO	Dimethyl sulfoxide
ECP	Ethyl 2-cyano-3-phenylacrylate
EDI	Edingtonite
EG	Ethylene glycol
EMT	Elf Mulhouse Number 2 (two)
F ⁻	Fluoride ion
FAU	Faujasite
FCC	Fluid catalytic cracking
FESEM	Field emission scanning electron microscope
FTIR	Fourier transform infrared
g	Gram
GC	Gas chromatography
GHz	Gigahertz
h	Hour
H ⁺	Proton
H ₂ O	Water
H ₃ BO ₃	Boric acid
HF	Hydrofluoric acid
HNO ₃	Nitric acid
HRTEM	High resolution transmission electron microscopy
ICP-OES	Inductively coupled plasma-optical emission spectrometry
IR	Infrared
IZA-SC	International Zeolite Association Structure Commission
kHz	Kilohertz
K ⁺	Potassium cation
KBr	Potassium bromide
K ₂ O	Potassium oxide
KOH	Potassium hydroxide
keV	Kiloelectronvolt

kV	Kilovolt
Li ⁺	Lithium cation
LIT	Lithosite
LTA	Linde Type A
LTF	Linde Zeolite-135 (one hundred and thirty-five)
LTJ	Linde Type J
LTL	Linde Type L
M	Molarity
MAS NMR	Magic angle spinning nuclear magnetic resonance
MEL	ZSM-11 (eleven)
MER	Merlinoite
MFI	ZSM-5 (five)
MHz	Megahertz
min	Minute
mL	Millilitre
mm	Millimetre
mmol	Millimol
MOR	Mordenite
ms	Millisecond
MS	Mass spectrometry
N ₂	Nitrogen molecule
Na ⁺	Sodium cation
Na ₂ CO ₃	Sodium carbonate
NH ₃	Ammonia
Na ₂ O	Sodium oxide
nm	Nanometre
NO	Nitric oxide
OH ⁻	Hydroxide ion
OSDA	Organic structure-directing agent
PBU	Primary building unit
PerBU	Periodic building unit
ppm	Part per million
PV-aided	Pervaporation-aided

RHO	Rho
rpm	Revolutions per minute
SAED	Selected area electron diffraction
SBU	Secondary building unit
SDA	Structure-directing agent
SEM	Scanning electron microscopy
Si	Silicon
SiC	Silicon carbide
SiO ₂	Silicon dioxide
SiO ₄	Silicon tetraoxide
SOD	Sodalite
SPE-MAS	Single pulse excitation magic angle spinning
t	Time
T	Temperature
<i>T</i>	Transmittance
TEAOH	Tetraethylammonium hydroxide
TEM	Transmission electron microscopy
TEOS	Tetraethylorthosilicate
TPD	Temperature-programmed desorption
W	Watt
XRD	X-ray diffraction

SINTESIS, PEMBENTUKAN DAN PENCIRIAN MANGKIN BES ZEOLIT JENIS W BERSKALA NANO

ABSTRAK

Zeolit W (topologi MER) merupakan zeolit yang sangat penting dalam industri pemangkinan dan pemisahan tetapi sintesisnya memerlukan agen pengarah struktur organik dan masa penghabluran yang panjang. Tujuan projek ini adalah untuk mensistesis dan mengkaji pembentukan zeolit W (topologi MER) bersaiz nano tanpa penggunaan agen pengarah struktur organik dalam masa penghabluran pendek selain menggunakannya sebagai mangkin heterogen untuk pelbagai tindak balas organik yang dimungkinkan dengan bes. Bahagian pertama memberi tumpuan kepada kajian mengenai kesan parameter sintesis seperti suhu pemanasan, masa tindak balas dan komposisi kimia hidrogel terhadap tingkah laku penghabluran zeolit W. Penemuan menunjukkan bahawa parameter sintesis mempunyai kesan yang ketara terhadap kadar penghabluran, ketulenan fasa zeolit, saiz zarah dan morfologi produk zeolit. Dengan menalakan parameter sintesis, zeolit W dengan empat morfologi yang berbeza (bentuk nanorod, seperti gandum, seperti peluru dan prismatic) dapat dihasilkan. Kajian lebih lanjut mengenai hubungan antara morfologi yang berbeza dan kebesan permukaan mendapati bahawa kebesan permukaan adalah berkadar linear dengan luas permukaan zeolit. Seterusnya, kajian proses penghabluran dan pertumbuhan hablur zeolit W bersaiz nano yang disintesis dengan abu daun buluh yang reaktif turut dilaporkan. Pelbagai teknik spektroskopi, mikroskopi dan analisis digunakan untuk mengikuti seluruh proses penghabluran tersebut. Zeolit W mengalami penyusunan semula fasa amorfus sebanyak dua kali sebelum berlakunya penukleusan, penghabluran dan pertumbuhan hablur. Zeolit W yang diperoleh mempunyai morfologi nanorod dan hablurnya cenderung menyusun secara selari untuk membentuk zarah sekunder yang

lebih besar. Akhir sekali, sintesis zeolit W nanohablur berliang meso hierarki melalui pemanasan gelombang mikro turut dibincangkan. Penghabluran cepat zeolit W bermorfologi nanorod yang unik ini dapat dicapai dalam masa 12 minit pada 180 °C dan hablur yang diperoleh mempunyai ukuran zarah kecil dengan ukuran sekitar $140 \times 17 \text{ nm}^2$. Kepentingan kation K^+ dalam mengarah pembentukan fasa zeolit MER juga telah dibukti. Nanohablur zeolit W yang disistesis seperti atas telah diuji dengan tiga model tindak balas organik yang dimungkinkan dengan bes, iaitu tindak balas sianoetilasi, tindak balas kondensasi Knoevenagel dan tindak balas Henry. Penemuan mendapati bahawa zeolit W dengan morfologi nanorod menunjukkan penukaran metanol yang tertinggi (94.1%) dalam tindak balas sianoetilasi kerana ia mempunyai luas permukaan tertinggi antara keempat-empat sampel berlainan morfologi. Selain itu, nanohablur zeolit ini juga menunjukkan prestasi yang tinggi dalam tindak balas kondensasi Knoevenagel antara benzaldehid dan etil sianoasetat dengan penukaran 84.3% dan keterpilihan yang jauh lebih baik (100%) daripada mangkin homogen manakala hablur nanozeolit berliang meso hierarki ini sangat aktif dalam tindak balas kondensasi Henry antara benzaldehid dan nitropropana, memberikan penukaran 90.2% dan keterpilihan 100% terhadap hasil primer. Secara kesimpulan, zeolit W berskala nano telah berjaya disintesis tanpa penggunaan agen pengarah struktur organik dalam masa penghabluran yang singkat dan zeolit ini menunjukkan potensi sebagai mangkin heterogen yang aktif dalam tindak balas bermungkinan bes.

SYNTHESIS, FORMATION AND CHARACTERIZATION OF NANOSCALE ZEOLITE TYPE W BASE CATALYST

ABSTRACT

Zeolite W (MER topology) is a very important zeolite in catalysis and separation industries but its synthesis requires the use of organic structure-directing agents (OSDAs) and long crystallization time. This project aims to synthesize and study the formation of nanosized zeolite W without organic structure-directing agent with shortened synthesis time while using it as heterogeneous catalyst for various base-catalyzed organic reactions. The first part focuses on studying the effect of the synthesis parameters such as heating temperature, reaction time and hydrogel chemical compositions on the crystallization behaviour of zeolite W. It is found that the synthesis parameters have significant impact on the crystallization rate, purity of the zeolite phase, particle size and morphology of the zeolite product. By tuning the synthesis parameters, zeolite W with four distinct morphologies (nanorods, sheaf-like, bullet-like and prismatic) can be obtained. Further investigation into the relationship between different morphologies and their surface basicity found that the surface basicity is linearly proportional to the surface area of the zeolites. Next, the time-dependent study on the nucleation and crystal growth process of nanosized zeolite W synthesized with reactive bamboo leaves ash (BLA) was reported. Various spectroscopic, microscopic and analytical techniques are used to follow the whole crystallization process. The zeolite undergoes amorphous phase reorganization twice before the occurrence of nucleation, crystallization and crystal growth. The zeolite W obtained exhibit nanorods morphology and tend to assemble in parallel forming bulkier bundle-like secondary particles. Lastly, the synthesis of nanocrystalline zeolite W with hierarchical mesoporosity under microwave heating condition was discussed.

Rapid crystallization of zeolite W with unique nanorods morphology was achieved within 12 min at 180 °C and the crystals obtained have small particle size at ca. $140 \times 17 \text{ nm}^2$. The importance of K^+ cations in directing the formation of MER zeolite phase has also been proven. The zeolite W nanocrystals synthesized above were tested with three model base catalyzed reactions, i.e. cyanoethylation reaction, Knoevenagel condensation reaction and Henry reaction. It is found that zeolite W with nanorod morphologies exhibits the highest catalytic conversion of methanol (94.1%) in cyanoethylation reaction since it has the highest surface area among the four morphologies. Besides, the zeolite W nanocrystals also gave excellent performance in Knoevenagel condensation reaction between benzaldehyde and ethyl cyanoacetate with 84.3% conversion and better selectivity (100%) than homogeneous catalysts whereas nanozeolite crystals with hierarchical mesoporosity are very active in Henry condensation reaction of benzaldehyde and nitropropane, giving 90.2% conversion and 100% selectivity towards primary product. In conclusion, nanosized zeolite W has been successfully synthesized without OSDA within a short crystallization time and the zeolite show promising use as an active heterogenous catalyst in base-catalyzed reactions.

CHAPTER 1

INTRODUCTION

1.1 General Introduction

Zeolites are crystalline microporous aluminosilicates made from $[\text{AlO}_4]^{3-}$ and $[\text{SiO}_4]^{4-}$ tetrahedral units which are linked together through the sharing of oxygen atoms to form three-dimensional open structures such as channels and cavities. The negative charge from the AlO_4 tetrahedron can be neutralized by the extra-framework cations (usually alkaline and alkaline-earth metal ions), creating a strong electrostatic field on the zeolite's surface (Ahmedzeki et al., 2016; Lee et al., 2012). Zeolites are widely used in catalysis, ion exchange, adsorption and separation processes due to their high porosity, tunable acidity/basicity and high ion-exchange capacity (Ahmedzeki et al., 2016; Lee et al., 2012).

In recent years, there has been much attention on the synthesis of zeolites with crystallite size below 100 nm (nanocrystalline zeolites) due to the growing interest in studying the nucleation and crystal growth of zeolites (Rakoczy and Traa, 2003). Nanocrystalline zeolites have a smaller crystal size in comparison to the conventional micrometer-sized zeolites (>1000 nm or >1 μm). This reduction in size has granted nanocrystalline zeolites several unique properties such as large external surface area, large pore volume, high hydrophilicity, high colloidal stability and the ability to reduce intracrystalline diffusion path lengths to the active sites (Wong et al., 2012; Muhammad et al., 2014). As a result, these distinctive properties have made nanocrystalline zeolites to have potentials in many applications including catalysts, adsorbents, lubricants, biosensors, thin films, holography and membranes

(Taufiqurrahmi et al., 2011; Cejka et al., 2016; Majano et al., 2011; Shan et al., 2006; Mintova et al., 2016).

Typically, zeolite nanocrystals are synthesized by an organic template approach in which the organic templates (amine, imidazolium or quaternary ammonium salts) are used as a structure-directing agent (SDA) and to control the crystallite size (Quirin et al., 1997; Barrett et al., 1998). The resulting solution are then heated under supersaturation condition to allow nucleation to take place more readily than crystal growth. So far, a number of zeolites, such as, BEA (Kamimura et al., 2010), FAU (Awala et al., 2015), MEL (Liu et al., 2008), MFI (Jiao et al., 2016), and MOR (Kurniawan et al., 2017) nanocrystals have been successfully synthesized. This traditional method, however, is not eco-friendly and hard to scale up due to the use of large amount of expensive and toxic organic structure-directing agents (OSDA). Furthermore, the use of normal oven heating, which is normally used for crystallization of zeolites, is high energy consuming, slow and inefficient in heating (Skoftefeld et al., 2000). In respect to this, OSDA-free system combined with microwave heating which provides low toxicity, fast, homogeneous and efficient heating are highly desirable in the context of green chemistry.

In OSDA-free method, the metal cations (e.g. Li^+ , Na^+ , K^+ , Ba^{2+} , Cs^+ , etc.) are added to the synthesis mixture as a template and a mineralizer to control the crystalline phase and the size of the final crystalline product. To date, six types of nanozeolites, namely SOD, EDI, FAU, LTL, LTA and LTJ, have been successfully prepared using this pathway (Fan et al., 2008; Wong et al., 2017a; Awala et al., 2015; Tan et al., 2015; Azizi et al., 2013; Ng et al., 2015b).

Potassium containing MER-type zeolite (or so-called zeolite K-W) with 8-ring pores and 3-dimensional channels is a very promising material in adsorption,

separation and catalysis involving small molecules due to its small pore size, unique framework properties and high hydrophilicity. However, the preparation of nanocrystalline zeolite K-W remains challenging due to the requirement of using large amount of OSDAs which are expensive and toxic to direct the formation of desired framework and to control the crystal size. Besides, this synthesis method also requires post-synthesis treatment such as calcination to remove the organic SDA from the pores which may lead to the partial collapse of zeolite structures (Mintova et al., 2013). Furthermore, the synthesis time is long (150 °C, 10 days), making scaling up the process in industry a difficult task. There are also inadequate literature detailing the microscopic and macroscopic examinations on nucleation and crystallization mechanism of the K-W zeolite. Thus, any new insight into the studies of nucleation and crystallization of zeolite K-W nanocrystals, particularly in the OSDA-free environment, is worthy of further investigation. In addition, there is also no thorough investigation into the catalytic behavior of K-W nanozeolite, particularly in base catalyzed reaction. Hence, any effort to elucidate the catalytic properties of this nanozeolite is also appreciated.

1.2 Research objectives

The objectives of this research are:

- a) To synthesize nanocrystalline K-W zeolite (<100 nm) without the use of OSDAs under conventional hydrothermal condition.
- b) To study effects/roles of initial chemical reactants (silica, alumina, KOH and water) and synthesis conditions (heating time and temperature) on the crystallization of K-W zeolite (crystallization kinetics, crystalline phase, morphology, topology).

- c) To synthesize K-W zeolite nanocrystals *via* OSDA-free pathway under microwave radiation condition.
- d) To study the crystallization process of nanocrystalline K-W zeolite through microscopic and spectroscopic methods.
- e) To investigate the catalytic behavior of K-W zeolite nanocrystals in base catalyzed reactions such as cyanoethylation between methanol and acrylonitrile, Knoevenagel condensation reaction between benzaldehyde and ethyl cyanoacetate and nitroaldol condensation reaction (Henry reaction) between benzaldehyde and nitropropane.

1.3 Scope of thesis

This thesis is divided into eight chapters, covering the background, experimental procedures and research outcomes of the project. Chapter 1 presents a brief introduction to the problem statements and research objectives of the project. Chapter 2 details the literature review focusing on the background and history of zeolites, applications of zeolites, zeolites syntheses, zeolite formation, fundamental concepts on microwave synthesis, and the catalytic reactions chosen for this project. Chapter 3 provides comprehensive experimental procedures that were carried out throughout the whole project, including the effect of synthesis parameters, the formation study of K-W nanocrystals, the microwave synthesis of nano-sized K-W zeolite, characterization of the zeolite samples and the catalytic behaviour study of K-W zeolite catalysts.

Chapter 4 reports the effect of synthesis parameters, such as the amount of starting raw materials, heating temperature and time, on the crystallization of K-W zeolites. X-ray diffraction (XRD) and scanning electron microscopy (SEM) were used

in this investigation. The explanation on the influence of the synthesis parameters on the crystallization of zeolite K-W were provided. In addition, the relationship between different crystal morphologies and their surface basicity were also investigated with carbon dioxide-temperature programmed desorption (CO₂-TPD) and nitrogen gas sorption analysis.

Chapter 5 elaborates on the synthesis of K-W zeolite nanocrystals using bamboo leaf ash (BLA) as silica source. The synthesis time was shortened with the use of BLA and the formation of zeolite crystals were studied using high resolution transmission electron microscopy (HRTEM). The change in chemical structure during the course of crystal formation were monitored using Fourier transform-infrared (FTIR) spectroscopy and solid-state magic angle spinning nuclear magnetic resonance (MAS NMR) spectroscopy. A plausible formation pathway was provided based on the experimental results.

Chapter 6 reports the synthesis of nano-sized K-W zeolite crystals using a novel structure-directing agent-free system *via* the microwave heating pathway. The zeolite crystals obtained was characterized with multiple techniques and instrumentations such as X-ray diffraction (XRD), Fourier transform infrared (FTIR) spectroscopy, transmission electron microscopy (TEM), scanning electron microscopy (SEM), nitrogen adsorption analysis and solid-state magic angle spinning nuclear magnetic resonance spectroscopy (MAS NMR).

Chapter 7 details the results and discussion on the catalytic behaviour of K-W nanocrystals as heterogeneous base catalyst in three model organic reactions, namely cyanoethylation reaction between methanol and acrylonitrile, Knoevenagel condensation reaction between benzaldehyde and ethyl cyanoacetate, and Henry reaction between benzaldehyde and nitropropane. Several aspects of the organic

reaction such as the effect of catalyst loading, effect of heating time and temperature, effect of reactants molar ratio, and effect of solvents were studied. Besides, the performance of K-W nanozeolite catalyst was compared with conventional homogeneous catalysts and catalyst reusability test was also conducted.

Lastly, chapter 8 is the conclusion of all the research findings. Suggestions for future works are also provided to promote further investigation into the potential applications of K-W zeolites and other discoveries in the field of zeolite science.

CHAPTER 2

LITERATURE REVIEW

2.1 Zeolites

Zeolites are a class of microporous aluminosilicate solids with a highly ordered crystal structure. The framework of zeolite consists of indefinitely extending $[\text{AlO}_4]^{3-}$ and $[\text{SiO}_4]^{4-}$ tetrahedral units linked to each other through the sharing of oxygen atoms forming three-dimensional open structures. The negative charge from the AlO_4 tetrahedron can be neutralized by the extra-framework cations (usually alkaline and alkaline-earth metal ions), creating a strong electrostatic field on the zeolite's surface (Figure 2.1) (Ahmedzeki, Yilmaz & Al-Tabbakh, 2016; Lee, Saad, Ng & Salleh, 2012).

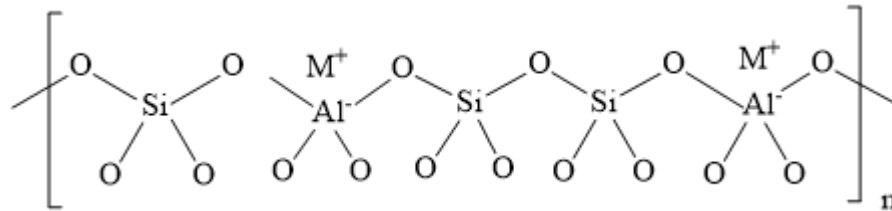


Figure 2.1 The chemical structure of zeolites whereby the negative charge on Al atoms is counter-balanced by the positive charge of metal cations.

Zeolites can be represented by the empirical formula based on the crystallographic unit cell shown in Equation 2.1 below:



where M represents the alkali or alkaline earth metal cations, n represents the cation valence, y is the number of tetrahedral per unit cell ranging from 2-200 and w represents the number of water molecules contained in the micropores of zeolites per unit cell (Petrov & Michalev, 2012).

The framework structures of zeolites are made up of primary building units (PBUs) and secondary building units (SBUs). The PBUs consist of TO_4 ($T = Si$ or Al) tetrahedra which are linked by sharing oxygen atoms to form a special arrangement of simple geometric forms called SBUs as shown in Figure 2.2 (Broach et al., 2012; Moshoeshoe et al., 2017).

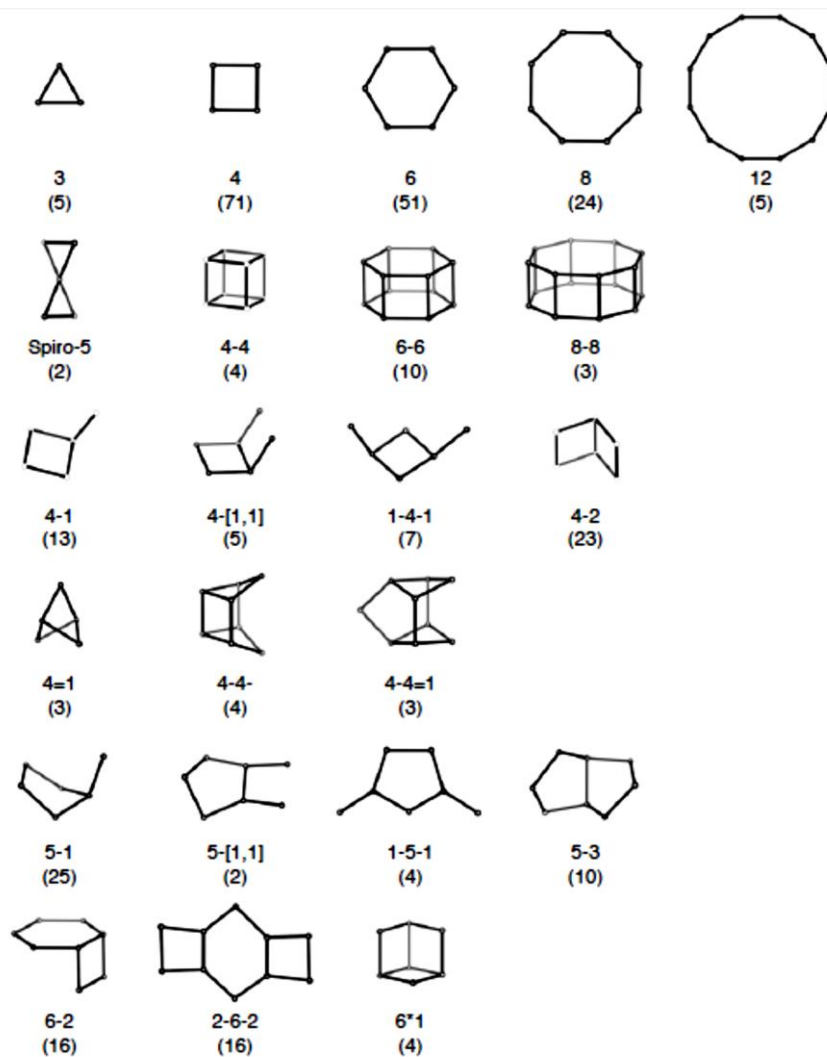


Figure 2.2 Secondary building units (SBUs) and their symbols. Number in parentheses indicates frequency of occurrence in zeolite frameworks (Moshoeshoe et al., 2017).

Apart from PBUs and SBUs, some zeolites may contain other components called composite building units (CBUs), such as double rings, cancrinite cages and alpha cavities. One of the most frequently encountered CBUs are the rings which are

characterised by the number of tetrahedrons contained. The most common zeolite rings found in zeolite frameworks are 4-, 5-, 6-, 8-, 10, and 12-membered rings. Zeolite rings of other sizes such as 3-, 7- 9-, 14-, 18-, 20- are relatively rare by comparison. Rings are sometimes joined to form more complex CBUs such as prisms and cages. Together, the SBUs and CBUs stack up and form the zeolite framework unique of its kind (Broach et al., 2012; Moshoeshoe et al., 2017).

The one-, two- or three-dimensional channels or interconnected voids of zeolite framework are normally occupied by the charge balancing cations and water molecules. The extra-framework cations are usually mobile and can undergo ion exchange. The water molecules, which may amount up to 50% of the zeolite crystals by volume, can be removed reversibly with heating, leaving an intact crystalline host structure with micropores (Flanigen, Broach & Wilson, 2010).

2.2 History of zeolites

The history of zeolites started with the discovery of mineral stilbite in 1756 by a Swedish mineralogist, Axel Fredrik Cronstedt. He categorized this new class of mineral as hydrated aluminosilicates of alkali and alkaline earths. He observed that upon heating stilbite in a blowpipe flame, the mineral experienced intumescence and released a significant amount of water. Hence, he coined the term “zeolite” for this type of mineral, which derived from the Greek words, *zeo* and *lithos*, meaning boiling and stone, respectively (Flanigen, 2001).

Since then, several scientists had reported on the properties of zeolite minerals. In 1840, Damour demonstrated that zeolites could be reversibly dehydrated while Eichhorn showed the ability of zeolite minerals to undergo cation exchange in 1858. In 1896, Friedel proposed the structure of dehydrated zeolites comprising of open

spongy framework after observing the occlusion of alcohol, benzene and chloroform by dehydrated zeolites. Similarly, in 1909, Grandjean demonstrated the ability of dehydrated chabazite to adsorb ammonia, air and hydrogen. The molecular sieve effect of zeolites was first reported by Weigel and Steinhoff in 1925 after observing that the dehydrated chabazite solids were able to adsorb water, methanol, ethanol and formic acid, but not ether, acetone or benzene (Flanigen, 2001).

In 1927, Leonard reported the first identification of zeolite minerals using X-ray diffraction method while Taylor and Pauling both described the crystal structures of analcime and sodalite in 1930, respectively. The synthesis of zeolites was pioneered by Barrer, who successfully reported the first synthetic mordenite zeolite in 1948. His work had inspired more investigations in zeolite synthesis, leading to the discovery of commercially important zeolites types A, X and Y by Milton and Breck (Reed & Breck, 1956; Milton, 1989).

To date, 248 types of zeolites have been synthesized in laboratories and approved by the International Zeolite Association Structure Commission (IZA-SC) while about 67 types of their naturally occurring counterparts have successfully been identified (Figure 2.3) (Baerlocher & McCusker, 2019). Naturally occurring zeolites often suffer from structural imperfections due to a variety of variables (e.g. impurity and cations) that can happen during their natural formations (Mondale, Carland & Aplan 1995), which results to their limited applications when the product purity is mattered. On the other hand, synthetic zeolites, being prepared in a controlled environment, have higher purity and a more uniform pore size distribution (Szostak, 1992). Hence, many synthetic zeolites, such as zeolites type X, Y, A and ZSM-5, possess the potentials to be applied industrially due to their distinct ion-exchange, adsorption and catalytic properties.

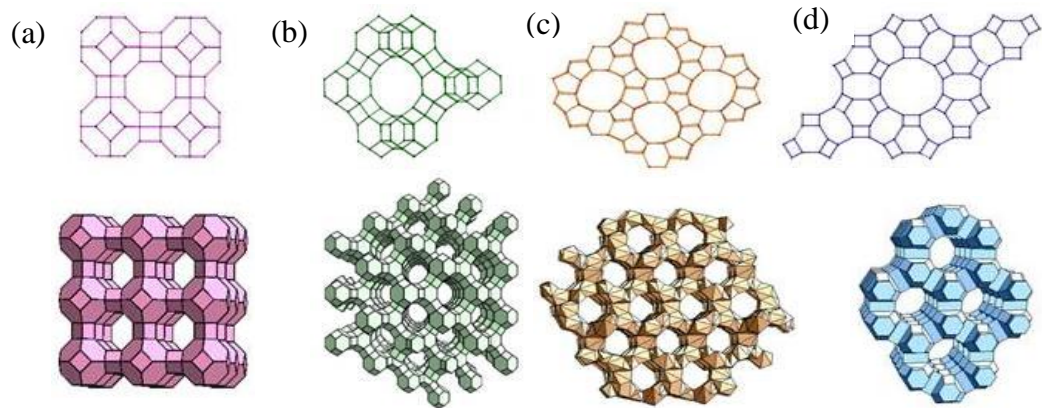


Figure 2.3 Examples of zeolites framework structures: (a) LTA, (b) FAU, (c) MFI and (d) LTL (Zheng et al., 2012).

2.3 Synthesis of zeolites

In general, the synthesis of zeolite involves the heating of a precursor gel which is made up of sources of T elements (T= Si, Al), structure-directing agent (SDA), mineralizer and solvent at a certain temperature and pressure. The type of zeolite framework formed, together with their morphological characteristics are greatly influenced by the synthesis parameters aforementioned.

2.3.1 Source of Si and Al

The most commonly used silica sources for zeolite synthesis are silica sol, tetraethylorthosilicate (TEOS), sodium silicate, fumed silica and amorphous silica. In certain cases, zeolites (Goel, Zones, & Iglesia, 2015), clays (Li et al., 2017) or volcanic glasses (Belviso, 2016) are utilized and recrystallized into the desired zeolites. Besides, zeolites synthesized using silica ashes from agricultural wastes such as rice husk and bamboo leaves have also been reported (Wong et al., 2018; Ng, et al., 2017). On the other hand, soluble aluminum sources, such as aluminum hydroxide, aluminum salts,

aluminum isopropoxide and sodium aluminate, are widely used in the preparation of zeolites. The sources and ratio of silica and alumina in the precursor gel not only can influence the growth kinetics of crystallizing zeolite but it may also promote the formation of a particular zeolite or affect the morphological properties of the final product (Valtchev & Mintova, 2009; Mohamed, Aly, El-Shahat, & Ibrahim, 2005; Salou, Kooli, Kiyozumi, & Mikamizu, 2001). The silica content in the zeolite framework determines its thermal stability, hydrophobicity/hydrophilicity, amount and distribution of active sites, and cation exchange capacity. Highly siliceous zeolites are progressively more hydrophobic as the silica content increases (Barrer, 1985). The introduction of Al^{3+} into the zeolite framework results in a negative charge which is then counter-balanced by the extra-framework cations captured in the channels and voids of the structure. Subsequently, a higher level of this substitution (smaller Si/Al ratio) offers a higher density of active sites and cation exchange capacity of a particular zeolite (Munthali, Elsheikh, Johan, & Matsue, 2014; Kraljević Pavelić et al., 2018).

2.3.2 Structure-directing agents (SDAs)

Sometimes, SDA is required to direct the formation of a zeolite framework and build the network of pores and cavities of the zeolite. There are two types of SDA, namely alkali metal cations and organic templates. Alkali metal cations and their hydration spheres function as the SDAs and usually they govern the formation of aluminous or low-silica zeolite frameworks (Valtchev & Mintova, 2009). A suitable alkali metal cation should be carefully chosen as the cation species may favour the formation of a certain zeolite type and the size of the cation itself may also affect the zeolite crystallization process heavily. For instance, Nearchou and Sartbaeva reported the synthesis of FAU zeolite with purely sodium cation as SDA and the progressive

substitution of sodium cation with caesium cation yielded RHO and ANA zeolite phases (Nearchou & Sartbaeva, 2015). Besides, a longer crystallization time was needed when the Na₂O in the synthesis system of zeolite A was partially replaced with K₂O, showing the structure breaking properties of a larger metal cation (Meise & Schwochow, 1973). On the other hand, the syntheses of highly siliceous zeolites (Si/Al > 10) usually require the use of organic structure-directing agents (OSDAs), such as alkylammonium hydroxides, arylammonium hydroxides, amines or alcohols which give templating effect that direct the formation of zeolite framework (Barrer, 1985). The use of organic template often results in pure zeolite phase and smaller crystals with narrower particle size distribution. However, the synthesis of zeolites with organic templates has many drawbacks such as environment-unfriendly, expensive, long crystallization time, low product yield and toxic (Ng, Delmotte, & Mintova, 2008; Song, Grassian, & Larsen, 2005). Besides, after the completion of synthesis process, an additional step of high temperature calcination is needed to remove the organic templates to open up the porosity of zeolites (Wang, H., Wang, Z., & Yan, 2000).

2.3.3 Mineralizer

In zeolite synthesis, the crystallization process is made possible by the use of mineralizer, whereby the reactants are converted into their soluble and reactive forms. The mineralizer increases the solubility of reactants, thus forming a super-saturated solution which significantly influences both the nucleation and crystallization processes. Similar to a catalyst, the mineralizer is not consumed during the reaction process but is released upon the completion of the crystallization reaction and then reuse in another new cycle (Weitkamp & Puppe, 1999). The most widely used

mineralizers in the synthesis of zeolites are hydroxide (OH^-) and fluoride (F^-) ions (Brice & Rudolph, 2007). The OH^- ions are usually employed in the syntheses of aluminum-rich zeolites which require high pH environments. The OH^- can be provided by the sources of Si and Al elements when the hydrolyzed silica and alumina solutions are used or by the alkali metal and organic SDA such as metal hydroxides and alkylammonium hydroxides, respectively. On the other hand, the F^- ions from fluoride salts or acids can be used as the mineralizer when a milder synthesis environment is needed ($\text{pH} < 10$), for instance in the synthesis of high-silica zeolite. In such environment, large crystals with fewer framework defects are obtained due to the lower supersaturation of the framework-forming species present in the synthesis mixture (Valtchev & Mintova, 2009; Qin et al., 2013).

2.3.4 Solvent

Generally, water is used as the solvent in a typical hydrothermal synthesis of zeolite as it can dissolve most of the reactants and intermediate species required for zeolite crystallization process. Besides taking part in templating the zeolite formation as hydration spheres with charged cations, it has also been shown that the amount of water in the synthesis system influences the type of framework formed as the crystallization process of different zeolites occur within a narrow range of pH (Valtchev & Mintova, 2009; Lechert, 2001). For example, NaY zeolite is synthesized at pH 11, while above this value, mordenite is crystallized and below this pH range, ZSM-5 is obtained (Lechert, 2001). Furthermore, the amount of water also affects the morphological properties of the final zeolite product. A lower water content means a higher concentration of reactants in the hydrogel which in turn increases the supersaturation condition of the mother liquor. A highly supersaturated hydrogel

promotes nucleation and less crystal growth. Hence, by reducing the water content, one can expect to obtain zeolite crystals with smaller particle size (Sashkina et al., 2017; Twomey et al., 1994).

2.4 Merlinoite zeolite

Zeolite W is a member in the MER (merlinoite) family. MER-type zeolite containing potassium cations was synthesized for the first time in 1953. However, it was not until 1977 that its natural counterpart, merlinoite, was discovered and identified (Donahoe & Liou, 1984).

2.4.1 Structure of MER framework

The secondary building units (SBUs) of MER framework consist of 4-, 8-membered ring and 8-8 double rings (D8R). These SBUs link among themselves to form the composite building units of MER framework as shown in Figure 2.4 (Baerlocher & McCusker, 2019).

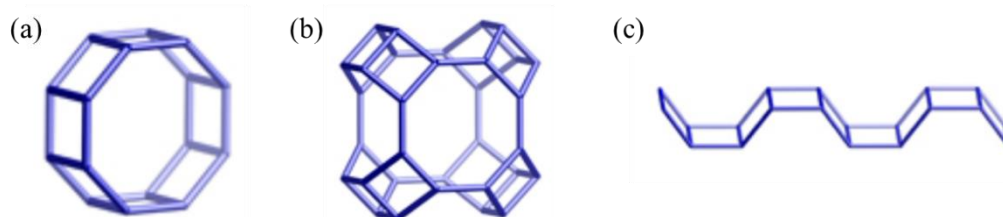


Figure 2.4 SBUs of MER framework: (a) double-8-ring (D8R), (b) pau unit and (c) double crankshaft chain (Baerlocher & McCusker, 2019).

MER-type framework structure consists of repeating units of crankshaft chains and each repeating unit is made up of four Si or Al tetrahedral species (Figure 2.5). When four crankshaft chains are connected to form an 8-ring channel, the periodic building unit (PerBU) of MER-type framework is obtained. The same PerBU can be

constructed from 4-fold D8Rs linked with each other as shown in Figure 2.6 (Baerlocher & McCusker, 2019).

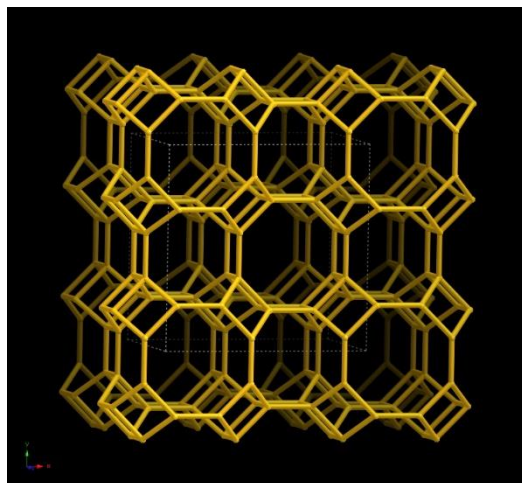


Figure 2.5 Framework structure of MER zeolite viewed along [001] (Baerlocher & McCusker, 2019).

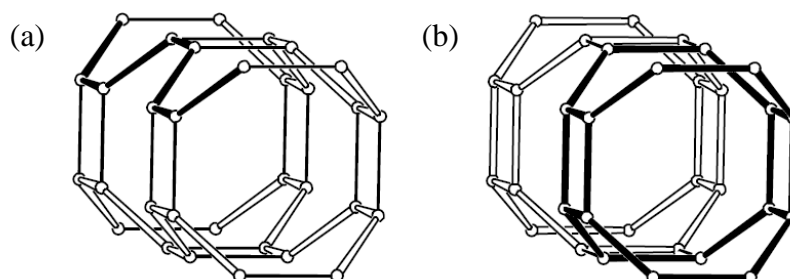


Figure 2.6 PerBU consisted of (a) 4 crankshaft chains and (b) 4-fold connected D8Rs (Baerlocher & McCusker, 2019).

Neighbouring PerBUs then connect to each other through the double crankshaft chains and form the *mer* cavities (Figure 2.7). The MER-type zeolite possesses four types of 8-membered ring channel systems, each with a diameter of $3.1 \times 3.5 \text{ \AA}^2$, $2.7 \times 3.6 \text{ \AA}^2$, $3.4 \times 5.1 \text{ \AA}^2$ and $3.3 \times 3.3 \text{ \AA}^2$ when viewed along [100], [010] and [001] planes for the latter two, respectively (Figure 2.8) (Baerlocher & McCusker, 2019).

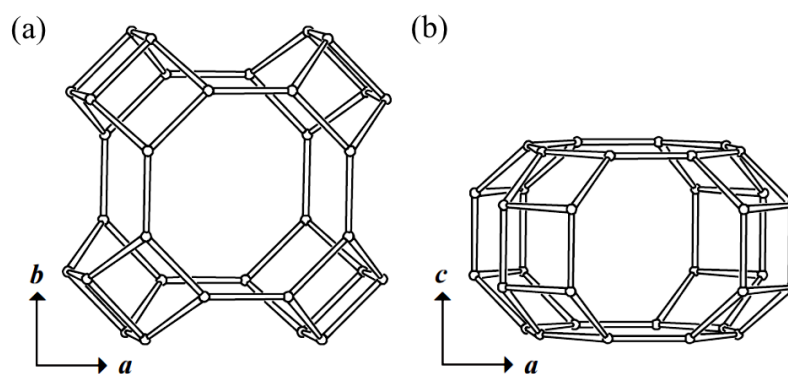


Figure 2.7 *mer* cavity (a) viewed along *c* direction and (b) viewed along *b* direction (Baerlocher & McCusker, 2019).

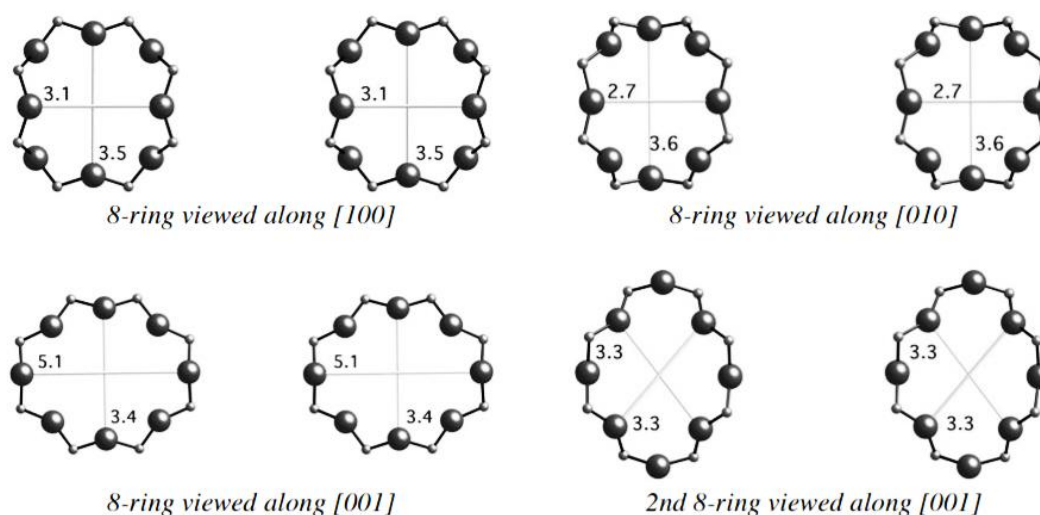


Figure 2.8 Four types of 8-membered ring channel systems in MER-type zeolite (Baerlocher & McCusker, 2019).

2.4.2 Synthesis of MER zeolite

Traditionally, organic structure-directing agents (SDAs) such as tetraethylammonium hydroxide (TEAOH), 1,6-diaminehexane and ethylene glycol (EG) are used in the synthesis of MER-type zeolite (Table 2.1). As seen from Table 2.1, the synthesis of zeolite MER requires long crystallization time, with the longest time and shortest time reported to be 14 days and 1 day, respectively. Besides, some attempts to obtain MER-type zeolite without using any organic templates have also

been successful (Quirin et al., 1997; Skofteland et al., 2001; Seo et al., 2010; Hou et al., 2012). However, all the zeolite crystals reported exhibit large crystal size and MER zeolite in nanometer scale is yet to be reported. Apart from that, the reported syntheses utilize traditional silica sources such as colloidal silica, tetramethyl orthosilicate and water glass in their experiments, which show a lack of investigation into using agricultural waste based silica such as rice husk ash or bamboo leave ash in zeolite synthesis.

Table 2.1 A comparison of MER zeolite synthesis conditions.

Precursor gel compositions	Heating conditions	References
Al ₂ O ₃ :35SiO ₂ :10.3Na ₂ O:4.9K ₂ O:3.5SDA ^a :1050H ₂ O	5 d, 140 °C	Quirin et al., 1997
Al ₂ O ₃ :29SiO ₂ :4.9Na ₂ O:19K ₂ O:400H ₂ O	2 d, 150 °C	
Al ₂ O ₃ :10SiO ₂ :1.4K ₂ O:4.4TEAOH ^b :150H ₂ O	14 d, 140 °C	Barrett et al., 1998
Al ₂ O ₃ :26.5SiO ₂ :13.3K ₂ O:26.5C ₆ H ₁₆ N ₂ ^c :3630.5H ₂ O	2 d, 165 °C	Thoma & Nenoff, 2000
Al ₂ O ₃ :5SiO ₂ :7.5K ₂ O:600H ₂ O	10 d, 150 °C	Skofteland et al., 2001
Al ₂ O ₃ :5SiO ₂ :2.5K ₂ O:11KNO ₃ :600H ₂ O		
Al ₂ O ₃ :6.4SiO ₂ :5.6K ₂ O:164.6H ₂ O	3 d, 165 °C	Seo et al., 2010
Al ₂ O ₃ :6.4SiO ₂ :5.6K ₂ O:0.64EG ^d :164.6H ₂ O		
Al ₂ O ₃ :10SiO ₂ :15K ₂ O:570H ₂ O	1 d, 150 °C	Hou et al., 2012
Aged for 10 h at room temperature		

^a6-methyl-1,3,3-trimethyl-6-azabicyclo[3.2.1]octane, ^btetraethylammonium hydroxide, ^c1,6-diaminohexane, ^dethylene glycol

2.4.3 Applications of MER zeolite

In the past decade, MER-type zeolite has successfully caught the attention of zeolite scientists in discovering its potential uses in various applications. Its high cation exchange capacity (CEC) is proven to be useful in the remediation of polluted water as it shows high efficacy in the adsorption of arsenic, cesium and strontium cations (Medina et al., 2010; Kakutani et al., 2017) while zeolite W, a zeolite with MER topology, has been used to extract K^+ cations from seawater (Hou et al., 2012; Jin et al., 2014). Besides, owing to its excellent CEC, potassium-bearing MER zeolite has the potential to be applied as potassium slow-release fertilizer extensively in nutrient-poor soil (Li et al., 2014; Flores et al., 2017). Apart from that, MER-type zeolite possesses 3-dimensional pore channel system which makes it a good candidate in the application of zeolite membrane. The first application of MER zeolite membrane is demonstrated in 2007 where the membrane was used for the dehydration of acetic acid solution (Nagase et al., 2007). Following this success, a MER zeolite membrane for pervaporation-aided (PV-aided) dehydration reaction process is then developed which allows for the stoichiometric ester condensation reactions at near room temperature (Inoue et al., 2007). MER zeolite membrane can also be used in the gas separation process of carbon dioxide and methane due to its high permeability and selectivity (Mirfendereski, 2019). Furthermore, MER zeolite is also used as an acidic heterogeneous catalyst in organic reactions such as dehydration of methanol and hydro-upgrading of fluid catalytic cracking (FCC) gasoline (Seo et al., 2010; Duan et al., 2015).

2.5 Nanoscale zeolites

Recently, the nanosized zeolite particles have been fascinating the world of science due to their unique properties and use in diverse fields including catalysis, membrane, photography, photonics, electronics, labelling, imaging, sensing, etc. (Wong et al., 2017a; Mintova et al., 2016; Ng et al., 2015b). Unlike conventional micron-sized zeolites, the reduction of zeolite size from micrometer to nanometer scale leads to substantial changes in their properties and thus, it is expected to provide materials with completely new properties (Mintova et al., 2015). While the chemical composition and the framework type structure of zeolites are important, the more vital factors are the size, shape and morphology of the nanoparticles that determine their catalytic, surface and colloidal properties. Different morphologies and sizes of the zeolite nanocrystals can be obtained from fine tuning of the synthesis parameters (e.g. initial gel composition, type of precursor materials, heating time and heating source, and temperature of preparation) in order to alter the induction, nucleation and crystal growth processes (Valtchev et al., 2005). Some nanocrystalline zeolites with open pore frameworks are shown in Figure 2.9.

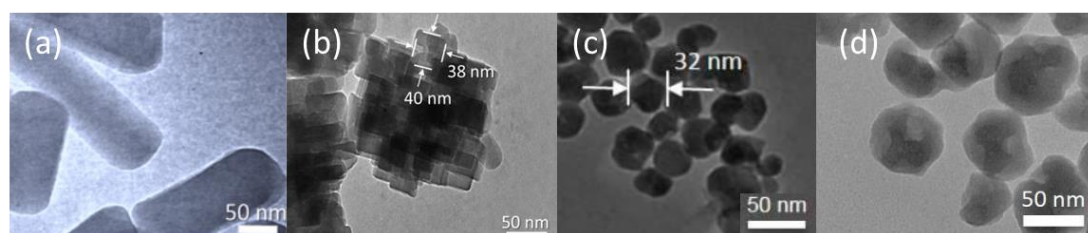


Figure 2.9 TEM images of (a) LTJ- (b) EDI- (c) ABW- and (d) ANA-type zeolite nanocrystals (Ng et al., 2015b; Wong et al., 2017a; Ghrear et al., 2019; Ng et al., 2019b).

2.5.1 Nanosized zeolites in membranes

The inherent properties of zeolites such as their tunable selectivity, high stability at high temperature, chemical and mechanical resistance, and catalytic activation make them promising separation membranes that could be used to separate small molecules (McLeary, Jansen and Kapteijin, 2006). Zeolite membranes separate molecular mixtures *via* molecular sieving, diffusion-controlled or adsorption-controlled permeation. Molecular sieving occurs when the molecular mixture has a dimension similar to the pore size or pore shape of zeolite. On the other hand, when the zeolite pore sizes are greatly larger than the molecules to be separated, the separation process can happen through the diffusion- or adsorption-controlled permeation mechanisms (Caro & Noack, 2008). For example, Cui and co-workers demonstrated the high selectivity for CO₂/CH₄ of zeolite T membrane due to molecular sieving effect (Cui, Kita and Okamoto, 2004) while the hydrophilic LTA zeolite membrane was used to separate water/alcohol mixtures through adsorption-driven permeation (Caro & Noack, 2008).

2.5.2 Nanosized zeolites in sensors

Zeolites have the potential to be applied in chemical sensing or detection owing to their flexible properties such as adjustable particle size, morphology and pore structure, high surface area, high adsorption capacity, mobile extra-framework cations and catalytic activity (Mintova, Gilson, & Valtchev, 2013). Zeolites can act as a main functional component in chemical sensors that depend on the adsorptive, conductive or catalytic properties of the zeolites and the interaction with analytes. They can also be the secondary or supplementary elements such as in the case of host-guest materials where the active sites are enclosed in the zeolite pores (Mintova, Jaber, & Valtchev,

2015; Xu, Wang, & Long, 2006). Besides that, nanosized zeolites are also a potential material used in enzyme-based sensors due to their large surface area with versatile surface properties such as modifiable surface charge, adjustable hydrophilicity/hydrophobicity and high dispersibility in organic and inorganic solutions. These characteristics resulted in their high adsorption capacity and the ability to immobilize enzymes or protein structures (Yu et al., 2006).

2.5.3 Nanosized zeolites in biological and medical applications

Several nanosized zeolites have been reported showing no or very low toxicity to human cells, for instance LTA (Kihara et al., 2011), LTL (Laurent et al., 2013), EMT (Laurent et al., 2013), FAU (Thomassen et al., 2012) and MFI (Bhattacharya, Naha, Naydenova, Mintova, & Byrne, 2012). Hence, there is a great interest in the utilization of nanoscale zeolites in biological and medical fields. As mentioned in Section 2.5.2, nanosized zeolites show great promise in immobilizing protein structures on their large external surfaces. Together with their micropores, textural mesopores and cavities which can confine a wide-range of drug molecules or contrasting agents, they are good candidates for a variety of drug delivery systems (Rimoli et al., 2008; Grund, Doussineau, Fischer, & Mohr, 2012; Al-Thawabeia & Hodali, 2015).

2.6 Synthesis of nanosized zeolites

In the early 90s, Schoeman and co-workers reported the first synthesis of nanosized zeolite crystals from a system called “clear suspensions” which contain discrete colloidal precursor particles. Several type of zeolites such as ZSM-2, FAU, LTA and SOD were synthesized from this method using organic SDAs (Schoeman et

al., 1994a; Schoeman et al., 1994b; Schoeman et al., 1995). SDAs are commonly used in the attempts of synthesizing nanoscale zeolites as they provide flexibility in the precursor gel chemical composition and produce highly pure zeolite product. However, the use of SDAs increases the production cost of zeolites since SDAs are expensive and in most cases, they are toxic. This synthesis method also requires post-synthesis treatment such as calcination to remove the organic SDA from the pores which may lead to the partial collapse of zeolite structures (Mintova et al., 2013).

To circumvent the drawbacks of SDAs mentioned above, zeolite scientists have started exploring the possibility of synthesizing nanoscale zeolites with precursor gel or suspension systems free of organic templates. This approach, however, could be applied only in the synthesis of low silica zeolites crystallizing from alkali metal rich precursor systems. A precursor system that provides abundant and uniform nucleation is very important in the formation of nanosized zeolite crystals. This system is usually chemically inhomogeneous due to the uncontrollable polymerization reaction between the Si and Al element species. Consequently, the chemical gradients in the hydrogel causes rapid diffusion in the system. Another key parameter in controlling the formation of nanosized zeolite is the heating temperature. Generally, a lower temperature favors nucleation over growth. A decrease in temperature also reduces Ostwald ripening, *viz.* a phenomenon where small crystals formed initially dissolve and redeposit on the surface of bigger crystals. As a result, smaller zeolite crystals with a more uniform particle size are obtained. After the completion of synthesis steps, the non-converted reactant species are separated by high-speed centrifugation. The purifying steps are repeated until pH 7 is reached and then the nanosized zeolites are redispersed in distilled water to prevent further particle agglomeration (Mintova et al., 2013; Mintova et al., 2015).

An example of such synthesis is the synthesis of nanosized K-F zeolite (EDI topology) by Wong and co-workers. The reported synthesis utilizes a very reactive gel system without organic SDAs and the crystallization of EDI nanocrystals were achieved within 3 h at 100 °C. The zeolite primary crystals exhibited cuboid shape morphology with very small crystallite size at ca. 27 nm and tend to agglomerate forming secondary spherical particles with particle size of ca. 310 nm (Figure 2.9b) (Wong et al., 2017a).

2.7 Zeolite formation mechanism

In recent years, much effort has been devoted to study the fundamental concept of zeolite crystallization mechanism in order to gain more control over the formation of zeolite phase and also the properties of zeolite synthesized. Generally, the zeolite crystallization process is initiated with the formation of discrete nuclei of a zeolite phase and then continues with the crystal growth process. Upon mixing the silica and alumina sources in basic medium, a clear suspension or a dense precursor gel is obtained where both systems contain monomeric silica, alumina and colloidal amorphous alumina silicates. When they are subjected to hydrothermal treatment, the contents of the precursor gel undergo reactions and convert into intermediates which then transform into the crystalline zeolite phase. Basically, the nucleation rate and crystal growth rate can be described as in Figure 2.10. The nucleation and growth of zeolites from two types of precursor systems are further described in the next sections.